JACS
JOURNAL OF THE AMERICAN CHEMICAL SOCIETY
Article
pubs.acs.org/JACS

Cell-Specific and pH-Activatable Rubyrin-Loaded Nanoparticles for Highly Selective Near-Infrared Photodynamic Therapy against Cancer

Jiangwei Tian,[†,§] Lin Ding,[†,§] Hai-Jun Xu,[‡] Zhen Shen,[‡] Huangxian Ju,*[,†] Li Jia,[†] Lei Bao,[†] and Jun-Sheng Yu*[,†]

[†]State Key Laboratory of Analytical Chemistry for Life Science and [‡]State Key Laboratory of Coordination Chemistry, School of Chemistry and Chemical Engineering, Nanjing University, Nanjing 210093, P.R. China

Supporting Information

ABSTRACT: Spatiotemporal control of singlet oxygen ($^1O_2$) release is a major challenge for photodynamic therapy (PDT) against cancer with high therapeutic efficacy and minimum side effects. Here a selenium-rubyrin ($NMe_2Se_4N_2$)-loaded nanoparticle functionalized with folate (FA) was designed and synthesized as an acidic pH-activatable targeted photosensitizer. The nanoparticles could specifically recognize cancer cells via the FA-FA receptor binding and were selectively taken up by cancer cells via receptor-mediated endocytosis to enter lysosomes, in which $NMe_2Se_4N_2$ was activated to produce $^1O_2$. The pH-controllable release of $^1O_2$ specially damaged the lysosomes and thus killed cancer cells in a lysosome-associated pathway. The introduction of selenium into the rubyrin core enhanced the $^1O_2$ generation efficiency due to the heavy atom effect, and the substitution of dimethylaminophenyl moiety at *meso*-position led to the pH-controllable activation of $NMe_2Se_4N_2$. Under near-infrared (NIR) irradiation, $NMe_2Se_4N_2$ possessed high singlet oxygen quantum yield (Φ_Δ) at an acidic pH (Φ_Δ = 0.69 at pH 5.0 at 635 nm) and could be deactivated at physiological pH (Φ_Δ = 0.06 at pH 7.4 at 635 nm). The subcellular location-confined pH-activatable photosensitization at NIR region and the cancer cell-targeting feature led to excellent capability to selectively kill cancer cells and prevent the damage to normal cells, which greatly lowered the side effects. Through intravenous injection of FA-$NMe_2Se_4N_2$ nanoparticles in tumor-bearing mice, tumor elimination was observed after NIR irradiation. This work presents a new paradigm for specific PDT against cancer and provides a new avenue for preparation of highly efficient photosensitizers.

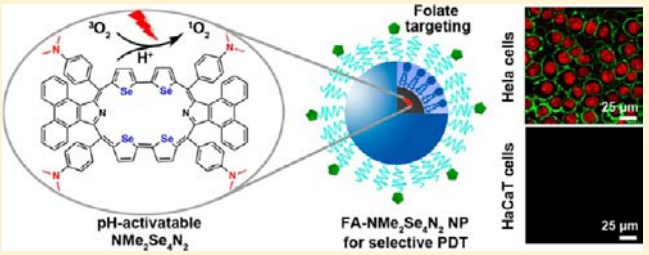

INTRODUCTION

Photodynamic therapy (PDT), which involves the combination of a photosensitizer, light, and molecular oxygen ($^3O_2$), is an emerging treatment modality for a variety of cancers.[1,2] Upon irradiation, the excited photosensitizer transfers energy to the surrounding $^3O_2$ to generate cytotoxic reactive oxygen species (ROS), especially singlet oxygen ($^1O_2$),[1a] resulting in irreversible damage of diseased cells and tissues.[2a,3] However, the clinic use of PDT is still limited due to the low selectivity of the currently available photosensitizers, which causes the treatment-related toxicity and side effects on adjacent normal tissues as well as prolonged skin photosensitization. To overcome this defect, the spatiotemporal control of $^1O_2$ release for controlling the PDT-induced cell death is an efficient way.[4] In other words, the photosensitizer should be deactivated in noncancerous tissues but can be activated by specific cancer-associated events to effectively produce $^1O_2$ in cancerous tissues, which permits high therapeutic efficacy against cancer and minimizes the side effects.

Due to the acidic tumor microenvironment (pH 6.5−6.8)[5] different from the normal tissues (7.4), the pH-activatable photosensitizers have attracted considerable interest.[6] The acidic extracellular environment induced by glycolysis under hypoxic conditions is perhaps the most pervasive tumor microenvironments, regardless of the tumor types or the developmental stages.[7] Compared with tumor-associated biomarkers, the bulky properties of the acidic tumor interstitium are easier to exert.[8] In addition, the significantly increased acidity in subcellular compartments of cancer cells such as lysosomes (pH 4.5−5.0)[9] further promotes the generation and release of $^1O_2$. Thus the pH-activatable photosensitizers provide a potential alternative strategy for selective PDT against cancer.

Recently several pH-activatable photosensitizers have been reported to produce cytotoxic reactive $^1O_2$ under irradiation.[6] Unfortunately, these photosensitizers lack the capability of selective localization in diseased cells, thus are not compatible with ex vivo or in vivo application. This motivates us to design pH-activatable PDT agents that can be accumulated in only

Received: August 9, 2013
Published: December 2, 2013

   dx.doi.org/10.1021/ja408286k | J. Am. Chem. Soc. 2013, 135, 18850−18858

Scheme 1. Schematic Illustration of (a) FA-$NMe_2Se_4N_2$ NPs for Selective PDT against Cancer; (b) Structure and Function of pH-Activatable $NMe_2Se_4N_2$ for $^1O_2$ Generation; and (c) Photophysical Process for pH-Activatable $^1O_2$ Generation of $NMe_2Se_4N_2$[a]

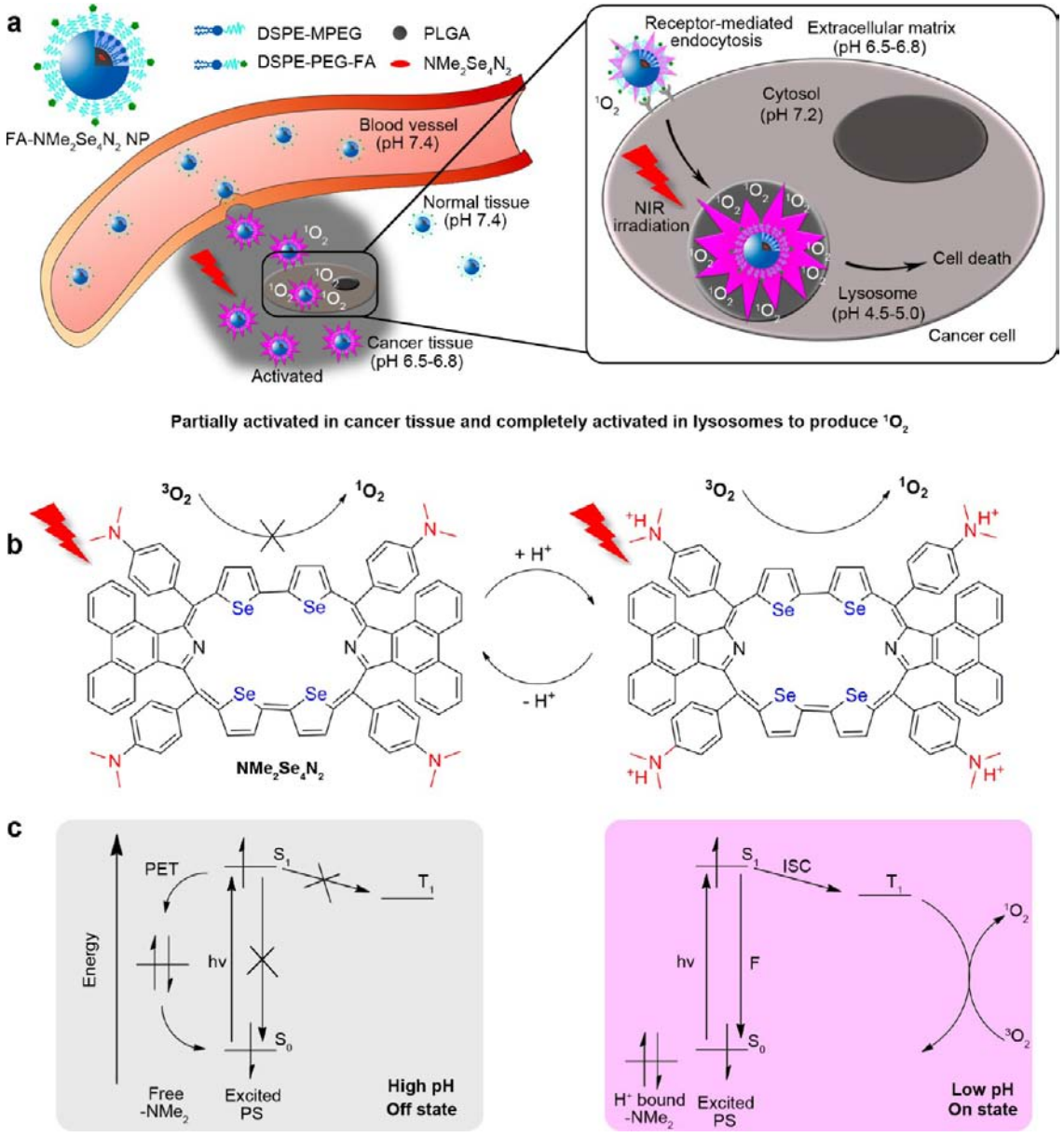

[a]S_0, singlet ground state; S_1, lowest singlet excited state; F, fluorescence; T_1, lowest triplet excited state; ISC, intersystem crossing; PET, photoinduced electron transfer; PS, photosensitizer.

cancer tissues and further taken up by cancer cells via receptor-mediated endocytosis for controllably producing $^1O_2$ in lysosomes to kill cancers. This work reports a cell-specific and acidic pH-avtivatable nanoparticle (FA-$NMe_2Se_4N_2$ NP) by introducing selenium into rubyrin core to enhance the $^1O_2$ generation efficiency, dimethylaminophenyl moiety at *meso*-position of rubyrin to achieve pH-controllable activity, and folate (FA) at the surface of nanoparticle to obtain cancer cell-targeting feature. As a highly efficient photosensitizer, the nanoparticles can generate $^1O_2$ in cancer tissues and lysosomes of cancer cells to induce cell death (Scheme 1a).

The folate receptor is generally overexpressed on the membrane of most cancer cells.[10] The presence of FA on the nanoparticles leads to the feature to specifically recognize cancer cells. The pH-activatable selenium-rubyrin ($NMe_2Se_4N_2$) shows strong absorption in near-infrared (NIR) region with a Soret band around 633 nm (λ_{Soret}) and two weak Q bands around 835 and 1156 nm (λ_Q). The $^1O_2$ release induced by $NMe_2Se_4N_2$ is "switched off" due to the efficient quenching of excited-state energy (S_1) by a fast photoinduced electron transfer (PET) process at physiological pH, whereas upon the protonation of N atom at acidic pH, the quenching process is rendered and the $^1O_2$ release is "switched on" (Scheme 1b,c). After the FA-$NMe_2Se_4N_2$ NPs are selectively taken up by cancer cells and accumulated in lysosomes via a FA receptor-mediated endocytosis, the acidic pH environment activates the FA-$NMe_2Se_4N_2$ NPs under NIR irradiation to produce $^1O_2$ and induce cell death in a lysosome-

dx.doi.org/10.1021/ja408286k | J. Am. Chem. Soc. 2013, 135, 18850−18858

associated pathway. The integrating utilization of FA and $NMe_2Se_4N_2$ leads to a significant enhancement of photodynamic selectivity to cancer. Using human cervical carcinoma Hela cells as model and immortalized human epidermal HaCaT cells as control, the newly designed photosensitizer was demonstrated to possess excellent capability to selectively kill cancer cells with low side effects. The new nanoparticles could be successfully used for highly efficient in vivo PDT under NIR irradiation.

EXPERIMENTAL SECTION

Materials and Reagents. Trifluorobonetherate ($BF_3{\cdot}Et_2O$), *N*,*N*,*N*′,*N*′-tetramethylethylenediamine (TMEDA), 1,3-diphenylisobenzofuran (DPBF), 2,3-dichloro-5,6-dicyano-1,4-benzoquinone (DDQ), methylene blue (MB), and other chemical reagents were purchased from Alfa Aesar (Ward Hill, MA, USA). Dry dichloromethane (CH_2Cl_2) was freshly distilled over CaH_2 under nitrogen. Dry *n*-hexane and tetrahydrofuran (THF) were distilled from sodium/benzophenone under nitrogen. Selenophene was distilled before use. Poly(D,L-lactide-*co*-glycolide) (PLGA, M_w: 5000, lactide:glycolide = 50:50), vitamin C, *N*-acetyl-*L*-cysteine (NAC), 3-(4,5-dimethylthiazol-2-yl)-2,5-diphenyltetrazolium bromide (MTT), indocyanine green (ICG), and 2′,7′-dichlorfluorescein-diacetate (DCFH-DA) were purchased from Sigma-Aldrich (St. Louis, MO, USA). Annexin V-FITC/propidium iodide (PI) cell apoptosis kit was obtained from KeyGen Biotech. Co. Ltd. (Nanjing, China). 1,2-Distearoyl-*sn*-glycero-3-phosphoethanolamine-*N*-[folate(poly ethylene glycol)-2000] (DSPE-PEG_{2000}-FA) and 1,2-distearoyl-*sn*-glycero-3-phosphoethanolamine-*N*-[methoxy (polyethylene glycol)-2000] (DSPE-$MPEG_{2000}$) were obtained from Avanti (Alabaster, AL, USA). LysoTracker Red was obtained from Invitrogen (Carlsbad, CA, USA). Ultrapure water was prepared using a Millipore Simplicity System (Millipore, Bedford, USA).

Characterization. ^{1}H NMR spectra were recorded with a Bruker 500 MHz spectrometer. MALDI-TOF-MS experiments were performed using an Applied Biosystems 4800 proteomics analyzer equipped with a Nd:YAG laser operating at 355 nm, a repetition rate of 200 Hz, and an acceleration voltage of 20 kV. UV−vis-NIR spectra were recorded on a SHIMADZU UV-3600 spectrophotometer. Steady-state fluorescence spectra were measured on an Edinburgh Instrument FLS-920 spectrometer. The morphology of the FA-$NMe_2Se_4N_2$ NP was characterized at a JEOL JEM-200CX transmission electron microscope (TEM) operated at 200 kV. The sample for TEM measurement was prepared by dropping the solution onto a carbon-coated copper grid following negative staining with 2.0% (w/v) phosphotungstic acid. The particle size and size distribution of FA-$NMe_2Se_4N_2$ NPs were measured by dynamic light scattering (DLS) using a Mastersizer 2000 particle size analyzer. Zeta potential measurement was performed at 25 °C on a Malvern Zeta Sizer-Nano Z instrument.

Synthesis of $NMe_2Se_4N_2$ and *t*$BuSe_4N_2$. $NMe_2Se_4N_2$ and the selenium-rubyrin with *tert*-butylphenyl moiety at the *meso*-position (*t*$BuSe_4N_2$) were synthesized according to the previous synthesis protocols[11] with some modifications as shown in Scheme 2. Synthetic experiments were carried out under an atmosphere of argon. *n*-Butylithium (*n*BuLi, 20 mL, 1.6 M solution in hexane, 32 mmol) was added to a solution of TMEDA (4.8 mL, 32 mmol) in dry *n*-hexane (52 mL), followed by addition of **1** (4.19 g, 16 mmol) under argon. The reaction mixture was heated under reflux for 1 h. After the reaction mixture was cooled to 0 °C in an ice bath, a solution of *p*-(dimethylamino)benzaldehyde (*p*-$NMe_2C_6H_4CHO$, 4.62 g, 31 mmol) or *p*-(*tert*-butyl)benzaldehyde (*p*-*t*BuC_6H_4CHO, 5.02 g, 31 mmol) in THF (32 mL) was added and stirred at 0 °C for 15 min. Afterward the solution was warmed to room temperature, and an ice-cold saturated NH_4Cl solution (50 mL) was added to stop the reaction. The reaction mixture was extracted with ether (3 × 50 mL). The organic layers were combined and washed with brine and dried over anhydrous Na_2SO_4. After removing the solvent under reduced pressure, the crude product was purified by column chromatography on silica gel using 20% ethyl acetate/petroleum ether as eluent to get **2**.

Scheme 2. Synthesis of $NMe_2Se_4N_2$ and *t*$BuSe_4N_2$

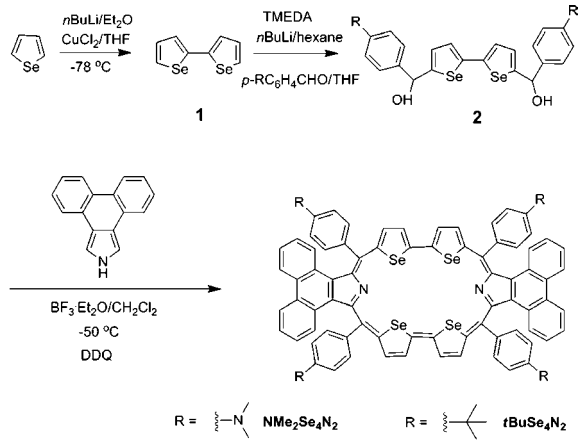

A solution of **2** (1 mmol) and phenanthro[9,10-*c*]pyrrole (217 mg, 1 mmol) in dry CH_2Cl_2 (60 mL) were condensed in the presence of a catalytic amount of $BF_3{\cdot}Et_2O$ (0.17 mL) under argon in the dark. The reaction mixture was stirred at −50 °C for 3 h and then warmed to room temperature. The reaction progress was monitored with UV−vis spectra. After the reaction was completed, DDQ (1 mmol, 227 mg) was added, and the mixture was stirred for another 12 h. The solvent was removed under reduced pressure, and the residue was purified by column chromatography on silica gel using a mixture of ethyl acetate and petroleum ether. After recrystallization from chloroform/methanol, the product of $NMe_2Se_4N_2$ or *t*$BuSe_4N_2$ was produced. ^{1}H NMR (500 MHz, DMF-d_7) of $NMe_2Se_4N_2$: δ = 9.17 (s, br, 4H), 8.82 (s, br, 6H), 8.52 (br, 8H), 7.97 (s, br, 6H), 7.71 (s, 6H), 7.44 (s, br, 10H), 3.56 (s, 24H). MALDI-TOF-MS: $[M + H]^+$ calcd for $C_{84}H_{64}N_6Se_4$, 1474.2951; found, 1474.2653. Anal. calcd (%) for $C_{84}H_{64}N_6Se_4$: C, 68.48; H, 4.38; N, 5.70; found: C 68.52; H 4.41; N 5.65. ^{1}H NMR (500 MHz, DMF-d_7) of *t*$BuSe_4N_2$: δ = 9.39 (s, br, 4H), 9.19 (s, br, 4H), 9.07 (d, 4H), 8.64 (s, br, 8H), 8.33 (d, 4H), 8.02 (d, 8H), 7.80 (m, 4H), 7.55 (m, 4H), 1.75 (s, 36H). MALDI-TOF-MS: $[M + H]^+$ calcd for $C_{92}H_{76}N_2Se_4$, 1526.4492; found, 1526.4797. Anal. calcd (%) for $C_{92}H_{76}N_2Se_4$: C, 72.44; H, 5.02; N, 1.84; found: C 72.50; H 5.08; N 1.88.

Synthesis of FA-$NMe_2Se_4N_2$ NPs. FA-$NMe_2Se_4N_2$ NPs were prepared via self-assembly of $NMe_2Se_4N_2$, PLGA, DSPE-$MPEG_{2000}$, and DSPE-PEG_{2000}-FA with a single-step sonication method.[12] Briefly, 0.8 mg $NMe_2Se_4N_2$ and 2.5 mg PLGA were dissolved in 1 mL CH_2Cl_2. DSPE-$MPEG_{2000}$/DSPE-PEG_{2000}-FA (8.5:1.5, molar ratio) with a total mass ratio of 15% to the PLGA polymer were added in 3 mL of 4% ethanol aqueous solution. The $NMe_2Se_4N_2$/PLGA solution was added dropwise under sonication using an ultrasonics processor (KUDOS, China) at a frequency of 35 kHz and power of 150 W for 5 min. Afterward, the solution was kept stirring for 4 h with protection from light at room temperature. The remaining organic solvent was removed in a rotary evaporator at reduced pressure at 30 °C. Finally, the FA-$NMe_2Se_4N_2$ NPs were centrifuged at 14 000 × *g* for 15 min, washed, and resuspended with ultrapure water and stored at 4 °C until use. Similar procedures were used to prepare the $NMe_2Se_4N_2$ NPs in the absence of FA and FA-*t*$BuSe_4N_2$ NPs. FA-$NMe_2Se_4N_2$/ICG NPs were prepared for investigating in vivo stability, pharmacokinetics, and biodistribution of the FA-$NMe_2Se_4N_2$ NPs by coencapsulating $NMe_2Se_4N_2$ and ICG into the nanocarrier.

Phototoxicity Assay. Hela cells (1×10^5) per well were seeded on 6-well plates or in 35 mm confocal dish (glass bottom dish) and incubated in complete medium for 24 h at 37 °C. The medium was then replaced with fresh culture medium containing 50 μg mL^{-1} FA-$NMe_2Se_4N_2$ NPs to incubate for 4 h at 37 °C. The cells were irradiated with a 635 nm laser at a power of 100 mW cm^{-2} for 100, 200, and 300 s, respectively. Afterward, the cells were stained with Annexin V-

dx.doi.org/10.1021/ja408286k | J. Am. Chem. Soc. 2013, 135, 18850−18858

FITC/PI according to the manufacturer's instruction, trypsinized, harvested, rinsed with PBS, resuspended, and subjected to perform flow cytometric assay using Cytomics FC500 Flow Cytometry (Beckman Coulter Ltd.). All experiments detected at least 10 000 cells, and the data were analyzed with FCS Express V3.

Cellular ROS Detection during Irradiation. After the Hela cells were incubated with FA-$NMe_2Se_4N_2$ NPs, they were further incubated with 10 μM DCFH-DA for 20 min and irradiated with a 635 nm laser at a power of 100 mW cm^{-2} for 0, 100, 200, or 300 s to perform the fluorescence detection of DCF with the flow cytometer, respectively, which could give the level of intracellular ROS.[13]

The irradiation-induced generation of ROS was also examined in the presence of vitamin C or NAC. After the FA-$NMe_2Se_4N_2$ NP-loaded cells were incubated with 2.5 mM vitamin C or NAC for 30 min and irradiated for 300 s, the cells were stained with Annexin V-FITC/PI to visualize the cell death with confocal laser scanning microscope (CLSM; TCS SP5, Leica, Germany).

The subcellular localization of ROS generated during irradiation was observed by staining the FA-$NMe_2Se_4N_2$ NP and then DCFH-DA-loaded Hela cells with LysoTracker Red for 10 min followed by irradiation using a 635 nm laser at a power of 100 mW cm^{-2} for 200 s. The colocalization of DCF and LysoTracker Red was performed with CLSM. DCF was excited at 488 nm with an argon ion laser, and the emission was collected from 505 to 555 nm. LysoTracker Red was excited at 543 nm with an argon ion laser, and the emission was collected from 570 to 680 nm. All images were digitized and analyzed by Leica Application Suite Advanced Fluorescence (LAS-AF) software.

Targeted PDT on Hela Cells. Hela or HaCaT cells were incubated with 50 μg mL^{-1} FA-$NMe_2Se_4N_2$ NPs for 4 h at 37 °C. The cells were irradiated with a 635 nm laser at a power of 100 mW cm^{-2} for 300 s. Afterward, the cells were stained with Annexin V-FITC/PI, and the cell death was visualized with CLSM.

Animals and Tumor Model. Specific pathogen-free female BALB/c nude mice, 5−6 weeks of age, were purchased from Shanghai Laboratory Animal Center, Chinese Academy of Sciences (SLACCAS) and bred in an axenic environment. All animal operations were in accord with institutional animal use and care regulations approved by the Model Animal Research Center of Nanjing University (MARC). Hela tumor model was established by subcutaneous injection of Hela cells (1×10^6) into the selected positions of the nude mice. During treatment, mice were anesthetized with 2.5% isoflurane in oxygen delivered at a flow rate of 1.5 L min^{-1}. Tumors were then allowed to grow to 4−5 mm in diameter. To determine the tumor volume, the greatest longitudinal diameter (length) and the greatest transverse diameter (width) of each tumor were determined using a vernier caliper, and the tumor volume was calculated using length × width^2 × 0.5.[14]

In Vivo Phototoxicity Assay on Subcutaneous Tumor Model. In vivo phototoxicity assay was performed using Hela tumor-bearing mice. The mice were subjected to four different treatments: group 1, untreated; group 2, laser only; group 3, intratumor injection of FA-$NMe_2Se_4N_2$ NPs only; group 4, intratumor injection of FA-$NMe_2Se_4N_2$ NPs combined with laser exposure. Each group contained 12 mice. 50 μL 0.5 mg mL^{-1} FA-$NMe_2Se_4N_2$ NPs in PBS was directly injected into the tumor mass of groups 3 and 4, respectively. Four h later, laser treatment was performed on groups 2 and 4 by irradiating the tumor region with an 808 nm laser at the power of 100 mW cm^{-2} for 30 min. Six mice were euthanized at 7 d post treatment, and tumor tissues of the above-mentioned treatment groups 1−4 were harvested for histological study by hematoxylin-eosin (H&E) staining under a BX51 optical microscope (Olympus, Japan) in a blinded fashion by a pathologist. The rest mice from the different treatment groups were monitored by measuring the tumor size using a vernier caliper for 12 d after the PDT treatment. The relative tumor volumes were calculated for each mouse as V/V_0 (V_0 was the tumor volume when the treatment was initiated).

Targeted PDT on Subcutaneous Tumor Model. Hela tumor-bearing mice were randomly divided into three groups, and each group contained six mice. They were performed the following treatments: group1, intravenous injection of PBS; group 2, intravenous injection of $NMe_2Se_4N_2$ NPs combined with irradiation; group 3, intravenous injection of FA-$NMe_2Se_4N_2$ NPs combined with irradiation. 100 μL PBS, 100 μL 0.5 mg mL^{-1} $NMe_2Se_4N_2$ NPs, or FA-$NMe_2Se_4N_2$ NPs in PBS were intravenously injected into groups 1−3. Eight h later, laser treatment was performed on groups 2, 3 by irradiating the tumor region with an 808 nm laser at a power of 100 mW cm^{-2} for 30 min. Tumor sizes were measured using a vernier caliper for 15 d after the PDT.

Statistical Analysis. Data were expressed as means ± SD from at least three experiments. Statistical analyses were carried out using a statistics program (GraphPad Prism; GraphPad Software). One-way ANOVA was used to compare the treatment effects. $P < 0.05$ was considered to be statistically significant.

RESULTS AND DISCUSSION

Design of pH-Activatable $NMe_2Se_4N_2$. As a highly efficient photosensitizer for in vivo PDT, it can be deactivated at physiological pH and has high singlet oxygen quantum yield (Φ_Δ) at acidic pH. Moreover, it should be activated under NIR light especially near 800 nm that is optimal for tissue penetration.[2a] The previous works have reported a series of fused-ring-expanded porphyrins with core modification and *meso*-aryl substitution[11,15] to display strong absorption in NIR region. Especially, the selenium-containing heterocyclic porphyrins display high Φ_Δ because of the heavy atom effect that enhances intersystem crossing (ISC) of the excited energy.[16] Therefore, this work designed a dimethylaminophenyl moiety at the *meso*-position of rubyrin to achieve pH-controllable feature and introduced selenium into rubyrin core to enhance the Φ_Δ (Scheme 1b). As comparison, an analogue rubyrin with *tert*-butylphenyl moiety at the *meso*-position (tBuSe$_4$N$_2$) was synthesized for studying the photophysical and photodynamic properties. Scheme 2 summarizes the synthesis routes of $NMe_2Se_4N_2$ and tBuSe$_4$N$_2$.

Photophysical and Photodynamic Properties of $NMe_2Se_4N_2$. The absorption spectrum of $NMe_2Se_4N_2$ displayed a Soret band at 633 nm with a high molar absorption coefficient ε of 2.21×10^5 M^{-1} cm^{-1} and two Q bands at 835 ($\varepsilon = 4.23 \times 10^4$ M^{-1} cm^{-1}) and 1156 nm ($\varepsilon = 1.21 \times 10^4$ M^{-1} cm^{-1}) (Figure S1), while tBuSe$_4$N$_2$ showed the absorption at 603 nm ($\varepsilon = 2.23 \times 10^5$ M^{-1} cm^{-1}), 723 nm ($\varepsilon = 3.67 \times 10^4$ M^{-1} cm^{-1}), and 1074 nm ($\varepsilon = 5.66 \times 10^3$ M^{-1} cm^{-1}) (Figure S2). Their Q bands are in NIR region. In response to the increasing H^+, $NMe_2Se_4N_2$ showed significantly increased fluorescence intensity (Figure 1a), corresponding to an increase in fluorescence quantum yield (Φ_F) from 0.16×10^{-3} at pH 7.4 to 5.6×10^{-3} at pH 5.0 (Table S1). In contrast, tBuSe$_4$N$_2$ showed a negligible fluorescence change at different pH with Φ_F change from 6.7×10^{-3} to 8.8×10^{-3} (Figure S3 and Table S1), indicating the contribution of the amine moiety (−NMe_2) as proton receptor to the pH response. The low Φ_F of $NMe_2Se_4N_2$ at high pH resulted from the PET quenching of S_1 by lone pair electrons of −NMe_2. Its protonation at acidic pH rendered the quenching process, leading to higher Φ_F.

The selectivity of $NMe_2Se_4N_2$ to H^+ over metal ions was also investigated by competition experiments. The fluorescence intensity of $NMe_2Se_4N_2$ displayed negligible variation in the absence or presence of excess K^+, Na^+, Ca^{2+}, Mg^{2+}, Zn^{2+}, Cu^{2+}, Fe^{2+}, and Hg^{2+} ions at pH 7.4 and pH 5.0 (Figure 1b), which indicated that $NMe_2Se_4N_2$ had high selectivity in response to H^+ in the presence of metal ions.

The production efficiency of $^1O_2$ induced by $NMe_2Se_4N_2$ and tBuSe$_4$N$_2$ under irradiation could be evaluated with the Φ_Δ, which was determined by a steady-state method using DPBF as

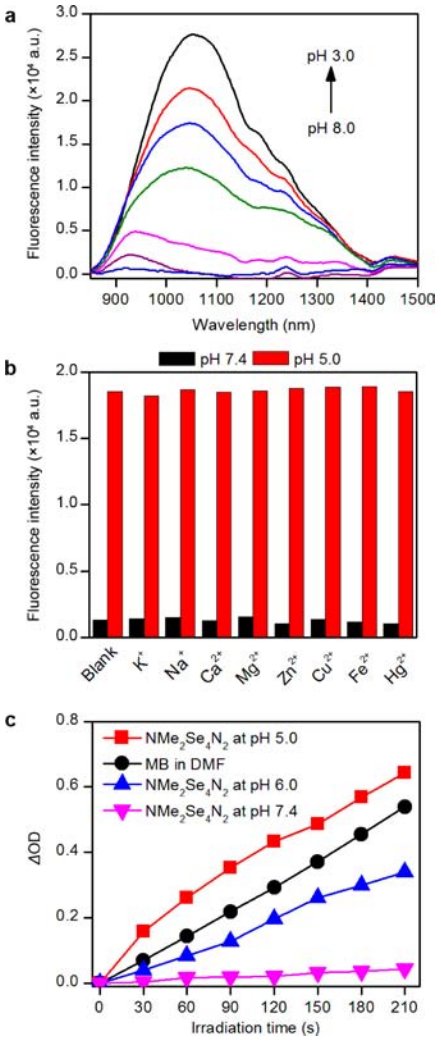

Figure 1. (a) Fuorescence emission spectra of 2 μM $NMe_2Se_4N_2$ in pH 8.0, 7.4, 6.5, 6.0, 5.0, 4.0, and 3.0 citrate buffer solutions containing 10% DMF (V/V) (λ_{ex} = 635 nm). (b) Effects of metal ions (100 μM) on fluorescence intensity of 2 μM $NMe_2Se_4N_2$ at pH 7.4 and 5.0. (c) Plots of change in optical density of DPBF at 418 nm vs irradiation time at 635 nm in pH 7.4, 6.0, and 5.0 citrate buffer solutions containing 10% DMF (V/V) and 2 μM $NMe_2Se_4N_2$ against MB in DMF as the standard.

the $^1O_2$ indicator and MB as the standard (Φ_Δ = 0.52) (Supporting Information).[17] The production efficiency for $NMe_2Se_4N_2$ was significantly dependent on solution pH (Figure 1c). It increased from 0.06 at pH 7.4 to 0.69 at pH 5.0 (Table S1), while the production efficiency for tBuSe$_4$N$_2$ was relatively stable with change from 0.47 at pH 7.4 to 0.54 at pH 5.0 (Figure S4 and Table S1). Therefore, it was reasonable to conclude that $NMe_2Se_4N_2$ allowed for pH-controllable $^1O_2$ release, and such a pH-responsive property was attributed to the presence of -NMe_2.

Characterization of FA-$NMe_2Se_4N_2$ NPs. In light of the low cytotoxcity, high transport efficiency, and stability of lipid-based materials,[12] a nanocarrier composed of DSPE-MPEG$_{2000}$, DSPE-PEG$_{2000}$-FA, and PLGA was fabricated via a self-assembly process to encapsulate $NMe_2Se_4N_2$ for its PDT application. The drug encapsulation efficiency of $NMe_2Se_4N_2$ was measured with UV−vis spectroscopy to be 48.8%. The TEM image of the resulting FA-$NMe_2Se_4N_2$ NPs showed well-dispersed spherical morphology (Figure S5). The average hydrodynamic diameter of the NPs measured by DLS was 152.3 ± 11.2 nm (Figure S6), which did not change for at least half of a month (Figure S7). The zeta potential of the FA-$NMe_2Se_4N_2$ NPs was observed to be −28.2 ± 4.5 mV (Figure S8), suggesting that the NPs were stable in aqueous medium.

Cytotoxicity of FA-$NMe_2Se_4N_2$ NPs. Low dark and strong light cytotoxicity are the necessary properties of the NPs for their application in PDT. The cytotoxicity of the FA-$NMe_2Se_4N_2$ NPs to Hela cells was examined in both the presence and absence of 635 nm irradiation using MTT assay (Figure S9). In the absence of light the FA-$NMe_2Se_4N_2$ NPs were basically noncytotoxic, while they exhibited high phototoxicity under irradiation of 30 J cm^{-2}. Furthermore, the phototoxicity increased along with the concentration of FA-$NMe_2Se_4N_2$ NPs with a half lethal dose (IC_{50}) of 35 μg mL^{-1} at an incubation of 4 h.

Annexin V-FITC together with PI has been widely used as fluorescent probe to distinguish viable cells from dead cells of different stages.[13] Therefore, the cell death induced by the FA-$NMe_2Se_4N_2$ NP-mediated PDT was examined with the dual fluorescence of Annexin V-FITC/PI using flow cytometry. The cell populations at different phases of cell death, namely, viable (AnnexinV-FITC$^-$/PI$^-$), early apoptotic (Annexin V-FITC$^+$/PI$^-$), and necrotic or late-stage apoptotic (Annexin V-FITC$^+$/PI$^+$) cells at different treatments were shown in Figure 2. After

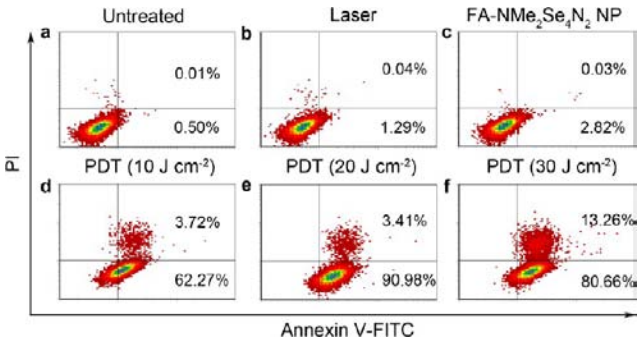

Figure 2. Flow cytometric analysis of Hela cell death induced by FA-$NMe_2Se_4N_2$ NP-mediated PDT.

the cells were treated with either laser or FA-$NMe_2Se_4N_2$ NPs alone, most of the cells are viable with a cell mortality rate <5% (Figure 2b,c), further demonstrating the low dark cytotoxicity. The cell mortality rate significantly increased upon the combining utilization of FA-$NMe_2Se_4N_2$ NPs and laser (Figure 2d−f), which was more than 90% at the light dose of 20 J cm^{-2}, suggesting the promising application of the FA-$NMe_2Se_4N_2$ NPs in PDT against cancer.

Contribution of ROS to PDT. To clarify the role of ROS in the FA-$NMe_2Se_4N_2$ NP-mediated PDT, the FA-$NMe_2Se_4N_2$ NP-loaded Hela cells were stained with DCFH-DA, a ROS probe, and vitamin C or NAC as ROS scavengers. DCFH-DA was nonfluorescent, its oxidized product by ROS (DCF) could emit a green fluorescence. Figure 3 shows the effect of irradiation on ROS generation in the cancer cells, which was detected with flow cytometry. Under irradiation, the FA-$NMe_2Se_4N_2$ NPs induced the production of ROS in Hela cells, and the amount of ROS was irradiation dose dependent. Vitamin C or NAC could efficiently prevent cell death (Figure 4), indicating the generated ROS in FA-$NMe_2Se_4N_2$ NP-mediated PDT was responsible for the cell death.

dx.doi.org/10.1021/ja408286k | J. Am. Chem. Soc. 2013, 135, 18850−18858

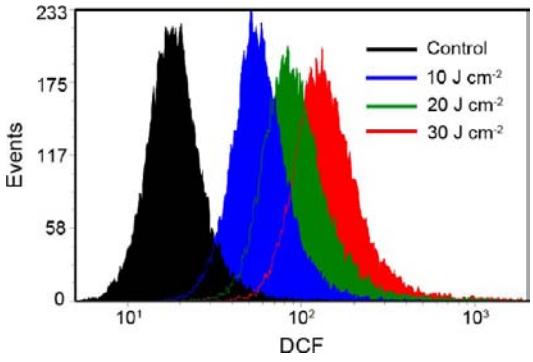

Figure 3. Flow cytometric detection of ROS generated during FA-$NMe_2Se_4N_2$ NP-mediated PDT with a ROS probe, DCFH-DA.

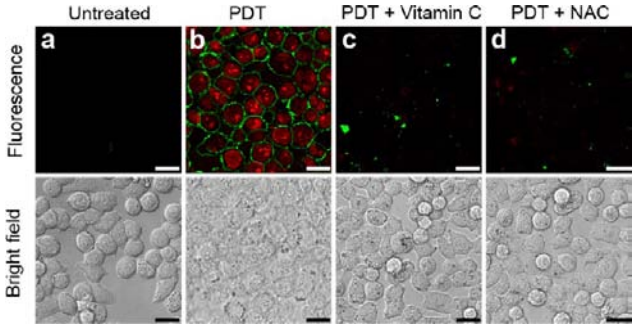

Figure 4. Confocal fluorescence images of Annexin V-FITC/PI stained Hela cells with different treatments. Scale bars: 25 μm.

Many evidence have suggested that intracellular ROS generation in different organelles induces cell death in different pathways.[18] For example, the ROS production in mitochondria leads to cell death in a mitochondrial apoptosis pathway such as cytochrome *c* release.[18c] Thus, the subcellular ROS localization was also investigated for elucidating the mechanism of FA-$NMe_2Se_4N_2$ NP-mediated PDT. Before irradiation, the Hela cells treated with FA-$NMe_2Se_4N_2$ NPs and then DCFH-DA showed negligible ROS generation, which was reflected by the unobservable fluorescence intensity of DCF (Figure 5a).

Upon irradiation the fluorescence of DCF was observed and well overlapped with the lysosomal tracker, LysoTracker Red (Figure 5b), indicating ROS was generated in lysosomes. This result suggested that the acidic pH environment (4.5−5.0) in lysosomes activated the FA-$NMe_2Se_4N_2$ NPs to produce ROS. Therefore, the cell death induced by the FA-$NMe_2Se_4N_2$ NP-mediated PDT involved a lysosome-associated pathway.[18d,e]

Selectivity of FA-$NMe_2Se_4N_2$ NPs. After Hela cells were incubated with $NMe_2Se_4N_2$ NPs, which were prepared with DSPE-$MPEG_{2000}$ in the absence of DSPE-PEG_{2000}-FA or FA-$NMe_2Se_4N_2$ NPs for 4 h and then irradiated with a 635 nm laser at a dose of 30 J cm^{-2}, the cells were stained with Annexin V-FITC/PI. The $NMe_2Se_4N_2$ NP-treated cells exhibited invisible fluorescence of Annexin V-FITC/PI, while the FA-$NMe_2Se_4N_2$ NP-treated cells displayed intense fluorescence with apoptotic characteristics (Figure S10), indicating significant cell death. Thus the presence of FA was also a key factor of the NP-mediated PDT. In the absence of FA, the NPs could not be uptaken into the cells. Contrarily, FA-$NMe_2Se_4N_2$ NPs could enter the cells via FA receptor-mediated endocytosis to be accumulated in lysosomes. The acidic pH environment activated the PDT activity of $NMe_2Se_4N_2$ and induced cell death.

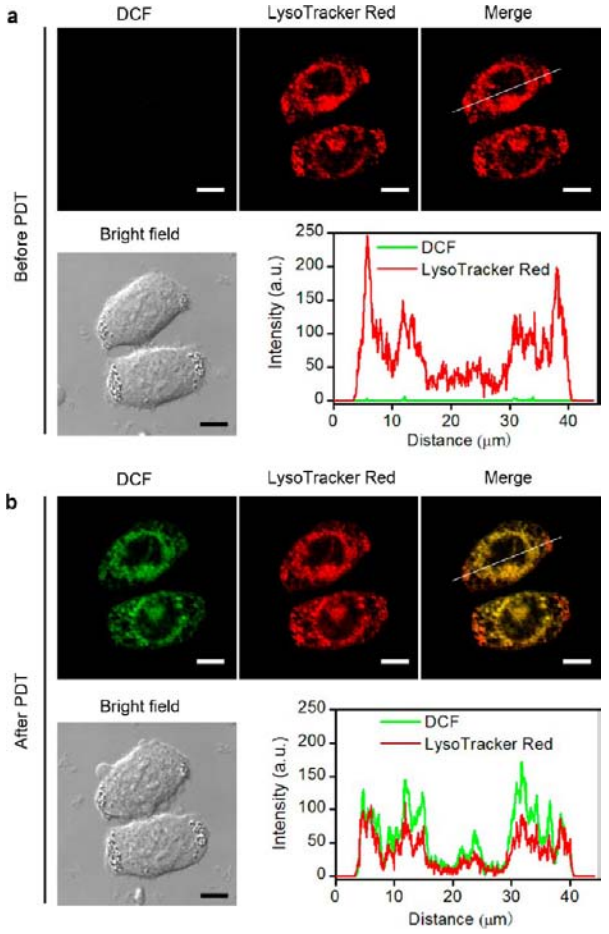

Figure 5. Subcellular localization of ROS generated during FA-$NMe_2Se_4N_2$ NP-mediated PDT by DCFH-DA and LysoTracker Red staining. (a) Control cells without irradiation. (b) Cells were incubated with 50 μg mL^{-1} FA-$NMe_2Se_4N_2$ NPs and exposed to 635 nm laser at 20 J cm^{-2}. Scale bars: 10 μm.

The FA receptor-mediated endocytosis led to the PDT selectivity to distinguish cancer from normal cells. Using Hela and HaCaT cells as model, the PDT selectivity was demonstrated (Figure 6). After incubation with FA-$NMe_2Se_4N_2$ NPs for 4 h, the cells were irradiated with a 635 nm laser and

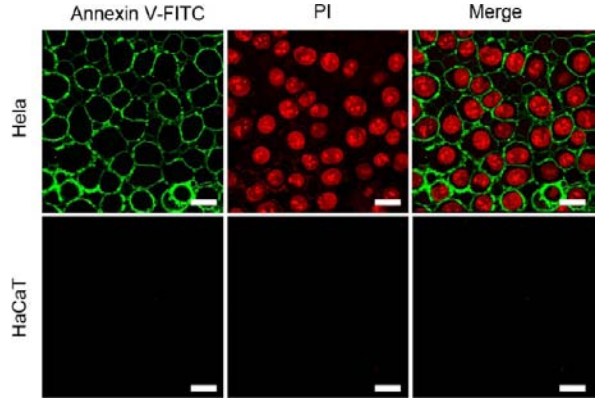

Figure 6. Confocal fluorescence images of Hela and HaCaT cells stained with Annexin V-FITC/PI after cells were incubated with 50 μg mL^{-1} FA-$NMe_2Se_4N_2$ NPs for 4 h and then exposed to a 635 nm laser at 30 J cm^{-2}. Scale bars: 25 μm.

dx.doi.org/10.1021/ja408286k | J. Am. Chem. Soc. 2013, 135, 18850−18858

then stained with Annexin V-FITC/PI. Only Hela cells showed strong apoptotic fluorescence, and the fluorescence from HaCaT cells was negligible. Thus FA-$NMe_2Se_4N_2$ NPs did not injure normal cells.

In Vivo PDT on Subcutaneous Hela Tumor-Bearing Mice. The in vivo phototoxicity of FA-$NMe_2Se_4N_2$ NPs to tumor was investigated in Hela tumor-bearing mice. Considering the efficient penetration depth of the irradiation, an 808 nm laser was employed to activate the FA-$NMe_2Se_4N_2$ NPs for in vivo PDT,[2a] which was different from 635 nm laser used in cell experiments. The tumors were subjected to four groups with different treatments. The phototoxicity of FA-$NMe_2Se_4N_2$ NP to tumor was assessed by monitoring their relative tumor volumes. After intratumor injection of FA-$NMe_2Se_4N_2$ NPs and laser exposure, tumor growth was almost completely inhibited, while no significant therapeutic effect was observed for intratumor injection or laser exposure alone (Figure 7a). The

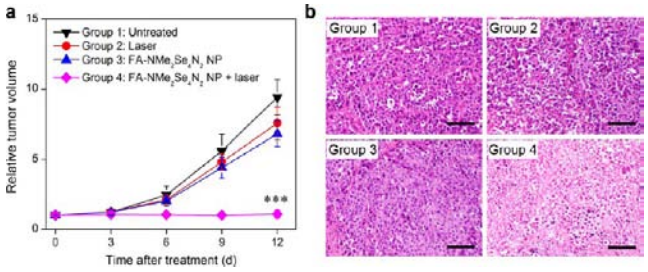

Figure 7. (a) Change of relative tumor volume (V/V_0) upon treatment with FA-$NMe_2Se_4N_2$ NPs or/and 808 nm laser at 100 mV cm^{-2} for 30 min. Data are means ± SD (6 mice per group), ***P < 0.001 compared to other groups using a one-way ANOVA. (b) H&E staining of tumor tissue sections from different treatment groups at 7 d after treatment. Scale bars: 100 μm.

treatment efficacy in term of tumor cell death was also evaluated by H&E staining on tissue sections from the different treatment groups at 7 d after treatment. Prominent necrosis was observed in histological sections from the group treated by PDT (Figure 7b), indicating the successful destruction of the tumor cells by the PDT with FA-$NMe_2Se_4N_2$ NPs. The tumor tissues without treatment and treated with laser or FA-$NMe_2Se_4N_2$ NPs alone showed indiscernible necrosis, revealing that FA-$NMe_2Se_4N_2$ NPs had little dark toxicity.

The targeted PDT efficacy was examined by intravenous injection of FA-$NMe_2Se_4N_2$ NPs in Hela tumor-bearing mice. The blood circulation profile of FA-$NMe_2Se_4N_2$/ICG NPs (Figure S11) gave a half-life ($t_{1/2}$) of 4.65 h, which indicated a long persistence of the NPs in bloodstream to corroborate their stability in vivo[19a] due to the presence of PEG and MPEG components.[19b,c] The FA-$NMe_2Se_4N_2$/ICG NPs could efficiently accumulate in Hela tumor within 8 h after intravenous injection and retain in the tumor even after 24 h post injection (Figure S12), while a negligible amount of the NPs was observed in liver, lung, and kidneys (Figure S13), indicating a targeted delivery of the NPs to tumor due to the presence of FA at their surface and FA receptors overexpressed on Hela cells.

The Hela tumor-bearing mice intravenously injected with FA-$NMe_2Se_4N_2$ NPs and then irradiated with a 808 nm laser showed a significant inhibition to tumor growth, compared to the mice treated with PBS or $NMe_2Se_4N_2$ NPs + irradiation (Figure 8). The relatively weaker antitumor effect of

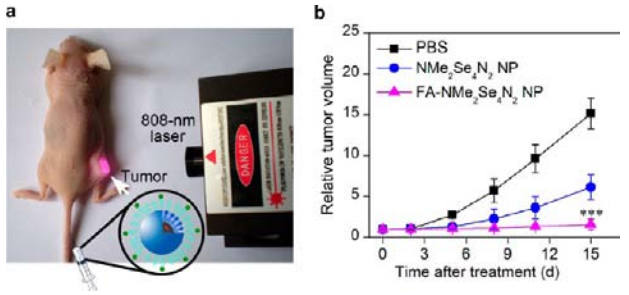

Figure 8. (a) Schematic illustration of targeted PDT on a Hela tumor-bearing mouse intravenously injected with FA-$NMe_2Se_4N_2$ NPs. (b) Change of relative tumor volume (V/V_0) after mice were intravenously injected with PBS, $NMe_2Se_4N_2$ NPs or FA-$NMe_2Se_4N_2$ NPs and irradiated with 808 nm laser at 100 mV cm^{-2} for 30 min. Data are means ± s.d. (6 mice per group), ***P < 0.001 compared to other groups using a one-way ANOVA.

$NMe_2Se_4N_2$ NPs suggested the importance of targeting properties. The $NMe_2Se_4N_2$ NPs could be activated only in extracellular matrix of tumor tissue to produce $^1O_2$, while FA-$NMe_2Se_4N_2$ NPs could be further activated to produce $^1O_2$ in the lysosomes with more acidic matrix via the FA receptor-mediated endocytosis. The targeting properties greatly improved the therapeutic efficacy of the PDT.

The potential in vivo toxicity or side effect is always a great concern for PDT agents used in medicine.[20] For verifying the practicability of the FA-$NMe_2Se_4N_2$ NPs, the mice treated with PDT at larger doses of FA-$NMe_2Se_4N_2$ NPs and irradiation were examined. The mice did not show significant body weight loss during 15 days after treatment (Figure S14). The slight weight loss of the PDT-treated mice could be attributed to the elimination of tumor tissue. At 30 day after the treatment, the tumors were completely eliminated, and the major organs were thus collected for histology analysis. No noticeable sign of organ damage or tumor metastasis was observed from H&E stained organ slices (Figure 9), suggesting the negligible side effects of FA-$NMe_2Se_4N_2$ NP for in vivo PDT. Moreover, pH-sensitive FA-$NMe_2Se_4N_2$ NP-treated mice showed significantly prolonged survival compared to pH-insensitive FA-tBuSe$_4N_2$ NPs (Figure S15), confirming the contribution of pH-activatable function. Notably, other acidic pH-activatable photosensitizers[6] can be easily encapsulated in the targeting NPs via similar self-assembly procedure for selective PDT, which will broaden the applications of this strategy to treat cancer.

■ CONCLUSION

We have synthesized a new photosensitized nanoparticle (FA-$NMe_2Se_4N_2$ NPs) to achieve selective and highly efficient PDT for cancer treatment by encapsulating newly designed $NMe_2Se_4N_2$ in the NPs. The $NMe_2Se_4N_2$ can act as an acidic pH-activatable photosensitizer for controllable $^1O_2$ release at NIR region. The introduction of selenium into rubyrin core enhances the $^1O_2$ generation efficiency, and the pH-controllable activity has been demonstrated to be due to the presence of dimethylaminophenyl moiety at *meso*-position of rubyrin. The FA conjugated on NP surface leads to the targeting properties to cancer cells. The FA-$NMe_2Se_4N_2$ NPs have little dark toxicity. Under irradiation FA-$NMe_2Se_4N_2$ NPs induce the production of $^1O_2$ in intracellular lysosomes to kill cancer cells and avoid the injure to normal cells. The NPs exhibit high efficiency for in vivo PDT without observable side effect.

dx.doi.org/10.1021/ja408286k | J. Am. Chem. Soc. 2013, 135, 18850−18858

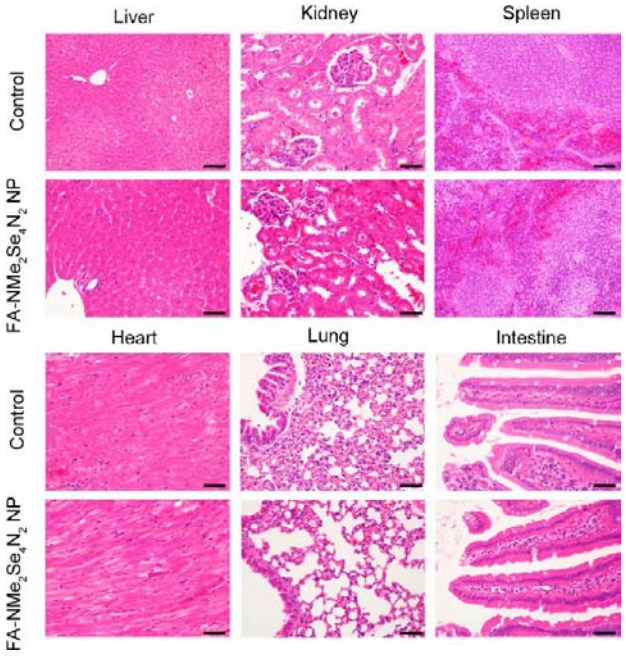

Figure 9. H&E stained images of tissue sections from different organs of mice with intravenous injection of FA-$NMe_2Se_4N_2$ NPs 30 days after PDT to eliminate tumors. Scale bars: 40 μm.

Overall, this work provides new insight into the design of smart PDT agents and new paradigm to achieve precise control of PDT performance at subcellular level, which promotes PDT to become a safer and more attractive clinical technique against cancer.

■ ASSOCIATED CONTENT

Supporting Information

Supplementary methods; absorption spectra of $NMe_2Se_4N_2$ and *t*$BuSe_4N_2$; pH dependence and $^1O_2$ production study of *t*$BuSe_4N_2$; TEM, DLS, zeta potential, MTT, blood circulation time and biodistribution assay of the FA-$NMe_2Se_4N_2$ NP; confocal imaging of the cell death induced by different NP-mediated PDT; relative mice body weight curves; survival rates of mice in different treatments. This material is available free of charge via the Internet at http://pubs.acs.org.

■ AUTHOR INFORMATION

Corresponding Authors

hxju@nju.edu.cn
jsyu@nju.edu.cn

Author Contributions

§These authors contributed equally.

Notes

The authors declare no competing financial interest.

■ ACKNOWLEDGMENTS

This study was supported by the National Basic Research Program (2010CB732400), National Science Fund for Creative Research Groups (21121091 and 21021062), National Natural Science Foundation of China (21322506, 21005037, 21135002, 91213301), and Ph.D. Fund for Young Teachers (20100091120034).

■ REFERENCES

(1) (a) Dougherty, T. J.; Gomer, C. J.; Henderson, B. W.; Jori, G.; Kessel, D.; Korbelik, M.; Moan, J.; Peng, Q. *J. Natl. Cancer Inst.* **1998**, *90*, 889−905. (b) Dolmans, D.; Fukumura, D.; Jain, R. K. *Nat. Rev. Cancer* **2003**, *3*, 380−387. (c) Brown, S. B.; Brown, E. A.; Walker, I. *Lancet Oncol.* **2004**, *5*, 497−508. (d) Chatterjee, D. K.; Fong, L. S.; Zhang, Y. *Adv. Drug Delivery Rev.* **2008**, *60*, 1627−1637. (e) Celli, J. P.; Spring, B. Q.; Rizvi, I.; Evans, C. L.; Samkoe, K. S.; Verma, S.; Pogue, B. W.; Hasan, T. *Chem. Rev.* **2010**, *110*, 2795−2838. (f) Master, A.; Livingston, M.; Sen Gupta, A. *J. Controlled Release* **2013**, *168*, 88−102.

(2) (a) Ethirajan, M.; Chen, Y.; Joshi, P.; Pandey, R. K. *Chem. Soc. Rev.* **2011**, *40*, 340−362. (b) Idris, N. M.; Gnanasammandhan, M. K.; Zhang, J.; Ho, P. C.; Mahendran, R.; Zhang, Y. *Nat. Med.* **2012**, *18*, 1580−1585. (c) Cui, S.; Yin, D.; Chen, Y.; Di, Y.; Chen, H.; Ma, Y.; Achilefu, S.; Gu, Y. *ACS Nano* **2012**, *7*, 676−688. (d) Cheng, Y.; C. Samia, A.; Meyers, J. D.; Panagopoulos, I.; Fei, B.; Burda, C. *J. Am. Chem. Soc.* **2008**, *130*, 10643−10647.

(3) (a) Kuimova, M. K.; Botchway, S. W.; Parker, A. W.; Balaz, M.; Collins, H. A.; Anderson, H. L.; Suhling, K.; Ogilby, P. R. *Nat. Chem.* **2009**, *1*, 69−73. (b) Niedre, M.; Patterson, M. S.; Wilson, B. C. *Photochem. Photobiol.* **2002**, *75*, 382−391.

(4) (a) Zheng, G.; Chen, J.; Stefflova, K.; Jarvi, M.; Li, H.; Wilson, B. C. *Proc. Natl. Acad. Sci. U.S.A.* **2007**, *104*, 8989−8994. (b) Koide, Y.; Urano, Y.; Yatsushige, A.; Hanaoka, K.; Terai, T.; Nagano, T. *J. Am. Chem. Soc.* **2009**, *131*, 6058−6059.

(5) (a) Tannock, I. F.; Rotin, D. *Cancer Res.* **1989**, *49*, 4373−4384. (b) Helmlinger, G.; Sckell, A.; Dellian, M.; Forbes, N. S.; Jain, R. K. *Clin. Cancer Res.* **2002**, *8*, 1284−1291. (c) Ganta, S.; Devalapally, H.; Shahiwala, A.; Amiji, M. *J. Controlled Release* **2008**, *126*, 187−204.

(6) (a) McDonnell, S. O.; Hall, M. J.; Allen, L. T.; Byrne, A.; Gallagher, W. M.; O'Shea, D. F. *J. Am. Chem. Soc.* **2005**, *127*, 16360−16361. (b) Ozlem, S.; Akkaya, E. U. *J. Am. Chem. Soc.* **2009**, *131*, 48−49. (c) Jiang, X. J.; Lo, P. C.; Yeung, S. L.; Fong, W. P.; Ng, D. K. P. *Chem. Commun.* **2010**, *46*, 3188−3190. (d) Zhu, X.; Lu, W.; Zhang, Y.; Reed, A.; Newton, B.; Fan, Z.; Yu, H.; Ray, P. C.; Gao, R. *Chem. Commun.* **2011**, *47*, 10311−10313. (e) Ke, M. R.; Ng, D. K. P.; Lo, P. C. *Chem. Commun.* **2012**, *48*, 9065−9067.

(7) Gatenby, R. A.; Gillies, R. J. *Nat. Rev. Cancer* **2004**, *4*, 891−899.

(8) Li, C.; Xia, J.; Wei, X.; Yan, H.; Si, Z.; Ju, S. *Adv. Funct. Mater.* **2010**, *20*, 2222−2230.

(9) (a) Su, J.; Chen, F.; Cryns, V. L.; Messersmith, P. B. *J. Am. Chem. Soc.* **2011**, *133*, 11850−11853. (b) Du, J. Z.; Du, X. J.; Mao, C. Q.; Wang, J. *J. Am. Chem. Soc.* **2011**, *133*, 17560−17563.

(10) (a) Xie, R.; Hong, S.; Feng, L.; Rong, J.; Chen, X. *J. Am. Chem. Soc.* **2012**, *134*, 9914−9917. (b) Santra, S.; Kaittanis, C.; Santiesteban, O. J.; Perez, J. M. *J. Am. Chem. Soc.* **2011**, *133*, 16680−16688.

(11) (a) Srinivasan, A.; V. G, A.; Narayanan, S. J.; Pushpan, S. K.; Kumar, M. R.; Chandrashekar, T. K.; Sugiura, K.i.; Sakata, Y. *J. Org. Chem.* **1999**, *64*, 8693−8697. (b) Wu, D.; Descalzo, A. B.; Weik, F.; Emmerling, F.; Shen, Z.; You, X. Z.; Rurack, K. *Angew. Chem., Int. Ed.* **2008**, *47*, 193−197.

(12) (a) Fang, R. H.; Aryal, S.; Hu, C. M.; Zhang, L. *Langmuir* **2010**, *26*, 16958−16962. (b) Zheng, C.; Zheng, M.; Gong, P.; Jia, D.; Zhang, P.; Shi, B.; Sheng, Z.; Ma, Y.; Cai, L. *Biomaterials* **2012**, *33*, 5603−5609. (c) Zheng, M.; Yue, C.; Ma, Y.; Gong, P.; Zhao, P.; Zheng, C.; Sheng, Z.; Zhang, P.; Wang, Z.; Cai, L. *ACS Nano* **2013**, *7*, 2056−2067.

(13) Thomas, A. P.; Saneesh Babu, P. S.; Asha Nair, S.; Ramakrishnan, S.; Ramaiah, D.; Chandrashekar, T. K.; Srinivasan, A.; Radhakrishna Pillai, M. *J. Med. Chem.* **2012**, *55*, 5110−5120.

(14) Euhus, D. M.; Hudd, C.; LaRegina, M. C.; Johnson, F. E. *J. Surg. Oncol.* **1986**, *31*, 229−234.

(15) (a) Xu, H. J.; Mack, J.; Wu, D.; Xue, Z. L.; Descalzo, A. B.; Rurack, K.; Kobayashi, N.; Shen, Z. *Chem.—Eur. J.* **2012**, *18*, 16844−16867. (b) Xu, H. J.; Mack, J.; Descalzo, A. B.; Shen, Z.; Kobayashi, N.; You, X. Z.; Rurack, K. *Chem.—Eur. J.* **2011**, *17*, 8965−8983.

(16) Ohulchanskyy, T. Y.; Donnelly, D. J.; Detty, M. R.; Prasad, P. N. *J. Phys. Chem. B* **2004**, *108*, 8668−8672.

(17) Adarsh, N.; Avirah, R. R.; Ramaiah, D. *Org. Lett.* **2010**, *12*, 5720−5723.
(18) (a) Buytaert, E.; Dewaele, M.; Agostinis, P. *Biochim. Biophys. Acta* **2007**, *1776*, 86−107. (b) Castano, A. P.; Demidova, T. N.; Hamblin, M. R. *Photodiagn. Photodyn. Ther.* **2004**, *1*, 279−293. (c) Lam, M.; Oleinick, N. L.; Nieminen, A. L. *J. Biol. Chem.* **2001**, *276*, 47379−47386. (d) Liu, L.; Zhang, Z.; Xing, D. *Free Radical Biol. Med.* **2011**, *51*, 53−68. (e) Repnik, U.; Stoka, V.; Turk, V.; Turk, B. *Biochim. Biophys. Acta* **2012**, *1824*, 22−33.
(19) (a) Poon, Z.; Lee, J. B.; Morton, S. W.; Hammond, P. T. *Nano Lett.* **2011**, *11*, 2096−2103. (b) Immordino, M. L.; Dosio, F.; Cattel, L. *Int. J. Nanomed.* **2006**, *1*, 297−315. (c) Wang, R. R.; Xiao, R. Z.; Zeng, Z. W.; Xu, L. L.; Wang, J. J. *Int. J. Nanomed.* **2012**, *7*, 4185−4198.
(20) (a) Yang, K.; Zhang, S.; Zhang, G.; Sun, X.; Lee, S. T.; Liu, Z. *Nano Lett.* **2010**, *10*, 3318−3323. (b) Cheng, L.; Yang, K.; Chen, Q.; Liu, Z. *ACS Nano* **2012**, *6*, 5605−5613.